https://doi.org/10.5194/amt-2020-349
Preprint. Discussion started: 18 September 2020

Atmospheric Measurement Techniques Discussions

Radiative transfer acceleration based on the Principal Component Analysis and Look-Up Table of corrections: Optimization and application to UV ozone profile retrievals

Juseon Bak[a#], Xiong Liu[a], Robert Spurr[b], Kai Yang[c],
Caroline R. Nowlan[a], Christopher Chan Miller[a], Gonzalo Gonzalez Abad[a],
and Kelly Chance[a]

[a]*Center for Astrophysics | Harvard & Smithsonian, Cambridge, MA, USA*
[b]*RT Solutions Inc., Cambridge, MA, USA*
[c]*Department of Atmospheric and Oceanic Science, University of Maryland College Park, College Park, Maryland, USA*
#Currently at Pusan National University, Busan, Korea

Abstract

In this work, we apply a principal component analysis (PCA)-based approach combined with look-up tables (LUTs) of corrections to accelerate the VLIDORT radiative transfer (RT) model used in the retrieval of ozone profiles from backscattered ultraviolet (UV) measurements by the Ozone Monitoring Instrument (OMI). The spectral binning scheme, which determines the accuracy and efficiency of the PCA–RT performance, is thoroughly optimized over the spectral range 265 to 360 nm with the assumption of a Rayleigh-scattering atmosphere above a Lambertian surface. The high level of accuracy (~ 0.03 %) is achieved from fast-PCA calculations of full radiances. In this approach, computationally expensive full multiple scattering (MS) calculations are limited to a small set of PCA-derived optical states, while fast single scattering and 2-stream multiple scattering calculations are performed, for every spectral point. The number of calls to the full MS model is only 51 in the application to OMI ozone profile retrievals with the fitting window of 270-330 nm where the RT model should be called at fine intervals (~0.03 nm with ~ 2000 wavelengths) to simulate OMI native measurements at 229 wavelengths (spectral resolution: 0.4-0.6 nm). We also developed a Look Up Table (LUT) to correct RT approximations performed using a scalar RT model with 4 streams (discrete ordinates) and 24 layers, thereby achieving the accuracy at the level attainable from simulations with a vector model with 12 streams and 72 layers; this speeds up the RT calculations by more than 2 orders of magnitude when ignoring other overhead. Overall, we speed up our OMI retrieval by a factor of 3.3 over the previous version, which has already been significantly sped up over line-by-line calculations due to various RT approximations. Improved treatments for RT approximation errors using LUT corrections improve

https://doi.org/10.5194/amt-2020-349
Preprint. Discussion started: 18 September 2020

Atmospheric Measurement Techniques Discussions

spectral fitting (2-5 %) and hence retrieval errors, especially for tropospheric ozone by up to ~10%; the remaining errors due to the forward model errors are within 5 % in the troposphere and 3 % in the stratosphere.

1. Introduction

Optimal estimation-based inversions have become standard for the retrieval of atmospheric ozone profiles from atmospheric chemistry UV-Vis backscatter instruments. This inversion model requires iterative simulations of not only radiances, but also of Jacobians with respect to atmospheric and surface variables, until the simulated radiances are sufficiently matched with the measured radiances. These ozone profile algorithms face a computational challenge for use in global processing of high spatial/temporal resolution satellite measurements, due to on-line radiative transfer (RT) computations at many spectral points from 270 to 330 nm; it is computationally very expensive to perform full multiple-scattering (MS) simulations with the polarized RT model. To reduce the computational cost, a scalar RT model can be applied together with a polarization correction scheme based on a LUT (Kroon et al., 2011; Miles et al., 2015). Another approach is to carry out on-line vector calculations at a few wavelengths (Liu et al., 2010) together with other approximations (e.g., low-stream, coarse vertical layering, Lambertian reflectance for surface and cloud, no aerosol treatment). However, the computational speed is still insufficient to process one day of measurements from the Aura Ozone Monitoring Instrument (OMI) within 24 h (30 cross-track pixels × 1644 along-track pixels × 14 orbits) with reasonable computational resources. Consequently, only 20 % of the available OMI pixels are processed to generate the operational ozone profile (OMO3PR) product (Kroon et al., 2011), and the spatial resolution is degraded by a factor of 4 to produce the research ozone profile (OMPROFOZ) product (Liu et al., 2010). With the advent of sophisticated inversion techniques and superior spaceborne remote sensing instruments, computational budgets have increased rapidly in recent years. Joint retrievals combining UV and thermal infrared (~ 9.6 um) have been investigated to better distinguish between upper- and lower-tropospheric ozone abundances from multiple instruments, e.g., OMI + TES, OMI +AIRS, and GOME-2 + IASI (Fu et al., 2013; 2018; Cuesta et al., 2013). The geostationary satellite instrument Tropospheric Emissions: Monitoring of Pollution (TEMPO), scheduled for Launch in 2022, is specially designed for joint retrievals combining UV and visible (540-740 nm) radiances to enhance the performance of retrievals for ground-level ozone (Zoogman et al., 2017). Moreover, the temporal and spatial resolutions of upcoming geostationary satellite instruments are being improved, leading to a tremendous increase in the data volume to be processed; for example, daily measurements of TEMPO (with ~2000 N/S cross-track pixels × ~1200 E/W mirror steps × ~8 times a day) are ~30 times greater in volume than those of OMI. Therefore, accelerating RT simulations is one of the highest priority tasks to assure operational capability. For speed-up, LUTs have often been used in trace gas retrieval algorithms to serve as proxies for RT modeling or to perform corrections to on-line RT approximations. In recent years, applying neural network techniques and principal component analysis (PCA) to RT computational performance has received quite a lot of attention (e.g., Natraj et al., 2005; Spurr et al., 2013;2016; Liu et al., 2016; Yang et al., 2016; Loyola et al., 2018; Nanda et al., 2019; Liu et al., 2020).

The goal of this paper is to improve both computational efficiency and accuracy of RT simulations in the OMI ozone profile algorithm (Liu et al., 2010) by combining a fast PCA-based RT model with two kinds of correction techniques. The application of PCA to RT simulations was first proposed by Natraj et al. (2005) by demonstrating a computational improvement of intensity simulation in the O_2 A band by a factor of 10 and with ~ 0.3 % accuracy compared to full line-by-line (LBL) calculations. This scheme has been deployed to the UV-backscatter, thermal emission, and cross-over régimes, and has been extended for the derivation of analytic Jacobians, for vector RT applications, and for bidirectional surface reflectances (Kopparla et al., 2016; 2017; Natraj et al., 2010; Somkuti et al., 2017; Spurr et al., 2013). The RT performance enhancement arises from a reduction in the number of expensive full multiple scattering calculations; the PCA scheme uses spectral binning of the wavelengths into several bins based on the similarity of their optical properties and the projection to every spectral point of these full MS calculations which are executed for a small number of PCA-derived optical states. In addition to the adaption of a PCA-based RTM for our ozone profile retrieval, we have adopted the undersampling correction from our previous implementation (Kim et al., 2009; Bak et al., 2019); this enables us to use fewer wavelengths for further speed-up without much loss of accuracy. Furthermore, we have developed a LUT-based correction to accelerate on-line RT simulations, by starting with a lower-accuracy configuration (scalar RT with no polarization, 4 streams, 24 layers) and then correcting the accuracy to the level attainable by means of a computationally more expensive configuration (vector RT, 12 streams, 72 layers). The stream value refers to the number of discrete ordinates in the full polar space; thus, for example, the term “12 streams” indicates the use of 6 upwelling and 6 downwelling polar cosine discrete ordinate directions. In previous work, PCA-based RT calculations were assessed mostly against LBL calculations, independently from the inverse model. Therefore, the PCA performance is likely to be overestimated in terms of operational capability, because operational algorithms have their own speed-up strategies with many approximations; this is the case for our ozone profile algorithm. As mentioned above, the PCA-based RT model is employed in this work to make forward-model simulations of OMI measurements for the retrieval of ozone profiles.

https://doi.org/10.5194/amt-2020-349
Preprint. Discussion started: 18 September 2020

Atmospheric Measurement Techniques
Discussions

Therefore, we evaluate the operational capability of our retrieval algorithm in terms of the retrieval efficiency as well as the accuracy, and assess these relative to the current operational implementation.

This paper is structured as follows. Section 2 describes the current forward model scheme and evaluates the approximations made in RT calculations, with the determination of the configuration parameters for accurate simulations. The updated forward model scheme is introduced for the PCA-based RT model in Section 3.1, and the two kinds of correction schemes to use less spectral sampling and less accurate RT configuration are detailed in Section 3.2. The evaluation is performed in Section 4 and then we summarize and discuss the results in Section 5.

2. Current forward model scheme based on Vector LIDORT (VLIDORT) only

We first describe the current v1 SAO OMI ozone profile algorithm that was implemented in OMI Science Investigator-led Processing Systems (SIPS) to generate the research OMPROFOZ ozone profile product, publicly available at the Aura Validation Data Center (AVDC, https://avdc.gsfc.nasa.gov/index.php?site=1620829979&id=74). It employs the OMI UV channel that is divided into UV1 (270-310 nm) and UV2 (310-380 nm). The spatial resolution of UV1 is degraded by a factor of 2 in order to increase the signal to noise ratio (SNR) in this spectral region. The full width at half maximum (FWHM) of the instrument spectral response function (ISRF) is ~0.63 nm for UV1 and ~0.42 nm for UV2, with corresponding spectral intervals of 0.33 nm and 0.14 nm, respectively. The total number of OMI wavelengths used in our spectral fitting for ozone profiles is 229, from 270-308 nm (UV1) and 312-330 nm (UV2). The RT model needs to simulate sun-normalized radiances as well as their derivatives with respect to the ozone profile elements and surface albedo. This simulation is iteratively performed to ingest the atmospheric and surface variables adjusted through the physical fitting between measured and simulated spectra and simultaneously the statistical fitting between the state vector and the *a priori* vector. The retrieval is optimized within typically 2-3 iterations (up to 10 is permitted). The vertical grids of the retrieved ozone profiles in 24 layers are initially spaced in log (pressure) at $P_i = 2^{-\frac{i}{2}}\,atm$ for 0 (surface), 23 (~55 km) and with the top of atmosphere set for P_{24} (~65 km). Each layer is thus approximately 2.5-km thick, except for the top layer (~ 10 km). A number of RT approximations have already been applied in the current forward model to speed up the processing. In the remainder of this section, the current forward model scheme is described, with its flow chart depicted in the left panel of Fig. 1. An error analysis is performed for optimizing the RT model configuration to maximize the simulation accuracy.

https://doi.org/10.5194/amt-2020-349
Preprint. Discussion started: 18 September 2020

Atmospheric Measurement Techniques Discussions
Open Access
EGU

In the first step, we select 93 effective wavelengths with variable sampling intervals, 1.0 nm below 295 nm, 0.4 nm from 295-310 nm, and 0.6 nm above 310 nm. The number of the wavelengths is smaller than the OMI native pixels (229 from 270-330 nm) by more than a factor of 2. The on-line radiative transfer model is run to generate the full radiance spectrum (single + multiple scattering) at these wavelengths in the scalar mode, with 8 streams and a Rayleigh atmosphere divided into 25 layers – a grid that is similar to that for the retrieval, except for the top layer (~ 55 km to 65 km) which is further divided into two layers. Note that the Vector Linearized Discrete Ordinate Radiative Transfer VLIDORT model Version 2.8 (Spurr and Christi, 2019) is implemented in this study. In step 2, a polarization correction is applied to the scalar calculations done in step 1 using the on-line vector calculation at fourteen wavelengths (visually shown with the vertical lines in Fig. 3.a.2). In step 3 the simulation at the effective wavelength grid is interpolated into 0.05 nm intervals with the undersampling correction, and the result is finally interpolated/convolved into OMI native grids in step 4.

Figure 2.b shows approximation errors related to undersampling from 0.02 nm to 0.1 nm compared to the simulated radiance at the sampling rate of the ozone cross sections (0.01 nm) (Fig. 2.a). This illustrates that current forward model calculation has trivial errors (less than 0.01 %) except for 0.02 % around 310 nm if there is no error after undersampling correction to 0.05 nm. The correction applied in step 3 allows relaxation of the sampling rate without loss of the accuracy. This correction is based on the adjustment of the radiance due to the difference of the optical depth profiles between fine (λ_h) and coarse (λ_c) spectral grids assisted by application of the weighting functions ($\frac{dI}{dx}$) as follows:

$$
\begin{aligned}
\mathrm{I}(\lambda_h) &= \mathrm{I}(\lambda_c) \\
&+ \sum_{l=1}^{N} \frac{\partial \mathrm{I}\ (\lambda_c)}{\partial \Delta_l^{gas}} \left(\Delta_l^{gas}(\lambda_h) - \Delta_l^{gas}(\lambda_c)\right) \\
&+ \frac{\partial \mathrm{I}\ (\lambda_c)}{\partial \Delta_l^{ray}} \left(\Delta_l^{ray}(\lambda_h) - \Delta_l^{ray}(\lambda_c)\right), \qquad (1)
\end{aligned}
$$

where Δ_l^{gas} and Δ_l^{ray} are the optical depth profiles for trace gas absorption and Rayleigh scattering, l = 1, $\cdots N_L$ (the number of atmospheric layers). Figure 2.c demonstrates that the undersampling correction works well for simulations at 0.2 nm intervals or less over the entire spectral range, but it can cause large errors when the simulations are performed at intervals of 1.0 nm, 0.4, and 0.6 nm for the spectral ranges, 270-295 nm, 295-310 nm, and 310-330 nm, respectively. Figure 3 shows the

Atmospheric Measurement Techniques
Discussions

approximations applied to on-line VLIDORT calculations, including (a.1) neglect of the polarization effect; (b) use of 8 streams; and (c) use of a coarse 24-layer height grid. As we mentioned above, in the v1 forward model the scalar model is used for all wavelengths, with the vector model at 14 wavelengths for correcting the scalar simulations. However, Figure 3.a.2 illustrates that second order of polarization correction errors (~0.2 %) could remain due to neglecting the dependence of polarization effects on the fine structures of ozone absorption. Using 8 streams causes errors of ~ 0.05 % above 320 nm, whereas using the 24 layers causes 1 % errors at shorter UV wavelengths. Based on the results shown in Fig 3, we conclude that there is room for improving the simulation accuracy by increasing the number of streams to 12, dividing the atmosphere into 72 layers and using more wavelengths in the polarization correction.

3. The improved forward model scheme based on PCA-VLIDORT

The right panel of Fig. 1.2 illustrates the flow chart of the new forward model scheme (v2) which employs the PCA-based RT model to perform on-line scalar simulations using 4 streams and a 24-layer atmosphere for RT performance enhancement (step 1) and two kinds of correction schemes for accounting for approximation errors (steps 2 and 3). Section 3.1.1 gives an overview on how the PCA tool is combined with the VLIDORT Version 2.8 model; full theoretical details may be found in Spurr et al. (2016) and Kopparla et al. (2017). Here, our paper gives details on how the PCA-based RT configuration is optimized for the application to UV ozone profile retrievals for maximizing the speed-up in the section 3.1.2. Section 3.2 specifies the step 2 wherein the LUT-based correction is applied to simulation errors due to the use of a scalar model, a smaller number of streams and coarser-resolution vertical grid. In the step 3 the undersampling correction is adopted from the v1 implementation, but the Rayleigh scattering term of the equation 1 is neglected for the speed up with trivial loss of accuracy.

3.1.1 General PCA procedure

The PCA-based RT process begins with a grouping of spectral points into several bins; atmospheric profile optical properties within each bin are similar. PCA is a mathematical transformation that converts a correlated mean-subtracted dataset into a series of principal components (PCs). To enhance RT performance, PCA is used to compress a binned set of correlated optical profile data into a small set of atmospheric profiles which capture the vast majority of the data variance within the bin. The layer extinction optical thickness Δ_{ni} and the single scattering albedos ω_{ni} are generally subjected to PCA, where n and i are indices for atmospheric layers ($n = 1, \cdots N_L$) and spectral points ($i = 1, \cdots N_S$),

https://doi.org/10.5194/amt-2020-349
Preprint. Discussion started: 18 September 2020

respectively. For each bin, the optical profiles $\{\ln\Delta_{ni}, \ln\omega_{ni}\}$ is composed of $2N_L \times N_S$ matrix G in log-space ($\mathrm{G}_{n,i} = \ln\Delta_{ni}$, $\mathrm{G}_{n+N_N,i} = \ln\omega_{ni}$). The mean-removed $2N_L \times 2N_L$ covariance matrix Y is then:

$$\mathrm{Y} = [\mathrm{G} - \langle\mathrm{G}\rangle]^{\mathrm{T}}[\mathrm{G} - \langle\mathrm{G}\rangle], \quad (2)$$

where <> denotes a mean-value over all grid points in a bin. This covariance matrix Y is decomposed into eigenvalues ρ_k and unit eigenvectors X_k through solution of the eigenvalue problem $\mathrm{YX}_k = \rho_k \mathrm{X}_k$. The scaled eigenvectors of the covariance matrix are defined as the empirical orthogonal function (EOFs), $W_k = \sqrt{\rho_k}\mathrm{X}_k$, where the index k is ranked from 1 to $2N_L$ in descending order staring with the largest eigenvalues. The principal components (PCs) are the projections of the original data onto the eigenvectors, $\mathrm{P}_k = \frac{1}{\sqrt{\rho_k}}\mathrm{G}W_k$. The original data set can then be expanded in terms of the mean value and a sum over all EOFs. As inputs to the RT simulation, the PCA-defined optical states are defined as $\mathrm{F}_\mathrm{o} = \exp[\langle\mathrm{G}\rangle]$ and $\mathrm{F}_k^{\pm} = \mathrm{F}_\mathrm{o}\exp[\pm\mathrm{W}_k]$, corresponding respectively to the mean value and to positive and negative perturbations from the mean value by an amount equal to the magnitude of k^{th} EOF. Therefore, $\Delta_{n,i}$ and $\omega_{n,i}$ (i=1…$\mathrm{N_S}$) are expressed as followings:

$$\mathrm{F}_o = \begin{Bmatrix}\Delta_{n,o} \\ \omega_{n,o}\end{Bmatrix} \equiv \begin{Bmatrix}\exp\left[\frac{1}{N_s}\sum_{i=1}^{N_s}\ln\Delta_{ni}\right] \\ \exp\left[\frac{1}{N_s}\sum_{i=1}^{N_s}\ln\omega_{ni}\right]\end{Bmatrix}; \ \mathrm{F}_k^{\pm} = \begin{Bmatrix}\Delta_{n,\pm k} \\ \omega_{n,\pm k}\end{Bmatrix} \equiv \begin{Bmatrix}\Delta_{n,o}\exp[\pm W_{n,k}] \\ \omega_{n,o}\exp[\pm W_{n+N_L,k}]\end{Bmatrix}. \quad (3)$$

For those optical quantities not included in the PCA reduction but still required in the RT simulations, the spectral mean values for the bin are assumed, as long as they have smooth monotonic spectral dependency or else are constant over the bin range. In our application, the phase functions and phase matrices for Rayleigh scattering are derived from bin-average values of the depolarization factor. Surface Lambertian albedos are constant in the RT simulation, but the calculated radiance is later adjusted to account for 1^{th} order wavelength dependency using surface albedo weighting functions. For larger bins, it is possible to include the depolarization ratio or the Lambertian albedo as additional elements in the optical data set subject to PCA; this has been investigated in another context by Somkuti et al. (2017).

In the PCA-based RT package, three independent RT models are combined in order to generate the full scattering intensity field ($\mathrm{I_{Full}}$) at each spectral point λ_i in a single bin

https://doi.org/10.5194/amt-2020-349
Preprint. Discussion started: 18 September 2020

$$\mathrm{I_{full}}(\lambda_i) \cong [\mathrm{I_{2s}}(\lambda_i) + \mathrm{I_{FO}}(\lambda_i)]C(\lambda_i). (4)$$

Two fast RT models, the "First-Order" (FO) and 2STREAM (2S), are used to generate an accurate single scatter (SS) field ($\mathrm{I_{FO}}$) and an approximate multiple scatter (MS) field ($\mathrm{I_{2S}}$), respectively, for every spectral point. The scalar 2S model computes the radiation field with 2 discrete ordinates only. To derive the correction factors $C(\lambda_i)$, we first compute (logarithmic) ratios of the full-scatter and 2S-based intensity fields calculated with PCA-derived optical states $\mathrm{F_o}$ and $\mathrm{F}_k^{\pm}$:

$$J_o = \ln\left[\frac{I_{VLD}(F_o) + I_{FO}(F_o)}{I_{2S}(F_o) + I_{FO}(F_o)}\right] \;; J_k^{\pm} = \left[\frac{I_{VLD}(\mathrm{F_k^{\pm}}) + I_{FO}(\mathrm{F_k^{\pm}})}{I_{2s}(\mathrm{F_k^{\pm}}) + I_{FO}(\mathrm{F_k^{\pm}})}\right]. \qquad (5)$$

Intensity ratios at the original spectral points $J(\lambda_i)$ are then obtained using a second-order central difference expansion based on the PCA principal components P_{ki}:

$$J(\lambda_i) = J_o + \sum_{k=1}^{N_{EOF}} \frac{(J_k^+ - J_k^-)}{2} P_{ki} + \frac{1}{2}\sum_{k=1}^{N_{EOF}} (J_k^+ - 2J_o + J_k^-)^2 P_{ki}^2 . \qquad (6)$$

The correction factors $C(\lambda_i) = \exp[J(\lambda_i)]$ are then applied to the approximate simulation $[\mathrm{I_{2s}}(\lambda_i) + \mathrm{I_{FO}}(\lambda_i)]$ according to Equation 4 above. More details can be found in the literature (Natraj et al., 2005, 2010; Spurr et al., ;2013; 2016; Kopparla et al., 2017).

So far, we have discussed generation of total *intensity* field, using values $\mathrm{I_{FO}}(\lambda_i)$ and $\mathrm{I_{2s}}(\lambda_i)$ from full-spectrum FO and 2S model calculation, and PCA-derived values $I_{VLD}(F)$, $I_{2S}(F)$ and $I_{FO}(F)$ based on PCA-derived optical states $F = \{F_o, \mathrm{F_k^{\pm}}\}$. The above procedure works with VLIDORT operating in scalar or vector mode; however, the 2S model is purely scalar, and cannot be used if we want to establish PCA-RT approximations to the Q and U components of the Stokes vector with polarization present. Instead, we rely on just the VLIDORT and FO models, and develop a PCA-RT scheme based on the differences between the VLIDORT and FO Q/U values for monochromatic and PCA-derived calculations, with an additive correction factor instead of the logarithmic ratios in Equation (6) above. This was first introduced in Natraj et al. (2010), and is discussed in detail in Spurr et al. (2016).

Of greater importance for us is the need to derive PCA-RT approximations to profile Jacobians (weighting functions of the total intensity with respect to ozone profile optical depths). A PCA-RT

https://doi.org/10.5194/amt-2020-349
Preprint. Discussion started: 18 September 2020

Jacobians scheme was developed by Spurr et al. (2013) for total column Jacobians in connection with the retrieval of total ozone; this scheme involved formal differentiation of the entire PCA-RT system as outlined above for the intensity field. This is satisfactory for bulk property Jacobians, but for profile Jacobians it is easier to write (Efremenko et al., 2014; Spurr et al., 2016):

$$\mathrm{K}^{(\xi)}_{Full}(\lambda_i) \cong \left[\mathrm{K}^{(\xi)}_{2S}(\lambda_i) + \mathrm{K}^{(\xi)}_{FO}(\lambda_i)\right] D^{(\xi)}(\lambda_i), \qquad (7)$$

Here, $\mathrm{K}^{(\xi)}_{2S}(\lambda_i) \equiv \frac{\partial \mathrm{I}_{2S}(\lambda_i)}{\partial \xi}$, with similar definitions for the FO and VLIDORT partial derivatives. The Jacobian correction factor $D^{(\xi)}(\lambda_i) = \exp[L^{(\xi)}(\lambda_i)]$ is determined using the same central-difference expansion as that in Equation (6), but with quantities

$$L^{(\xi)}_0 = \ln\left[\frac{\mathrm{K}^{(\xi)}_{VLD}(F_o) + \mathrm{K}^{(\xi)}_{FO}(F_o)}{\mathrm{K}^{(\xi)}_{2S}(F_o) + \mathrm{K}^{(\xi)}_{FO}(F_o)}\right] \; ; L^{(\xi)}_{\pm k} = \left[\frac{\mathrm{K}^{(\xi)}_{VLD}(\mathrm{F}^{\pm}_{\mathrm{k}}) + \mathrm{K}^{(\xi)}_{FO}(\mathrm{F}^{\pm}_{\mathrm{k}})}{\mathrm{K}^{(\xi)}_{2S}(\mathrm{F}^{\pm}_{\mathrm{k}}) + \mathrm{K}^{(\xi)}_{FO}(\mathrm{F}^{\pm}_{\mathrm{k}})}\right] \qquad (8)$$

in place of J_o and $J^{\pm}_k$ in Equation (5).

3.1.2 The binning scheme

The major performance saving is achieved by limiting full-MS VLIDORT calculations to those based on the reduced set of PCA-derived optical states $\mathrm{F_o}$ and $\mathrm{F}^{\pm}_k$. A general binning scheme has been developed over the shortwave region from 0.29 to 3.0 μm (Kopparla et al. 2016), whereby the entire region is divided into 33 specially-chosen sub-windows encompassing the major trace-gas absorption signatures; in each such sub-window there are 11 bins for grouping optical properties, and up to four EOFs for each PCA bin treatment; with this scheme, radiance accuracies of 0.1% can be achieved throughout the region. However, the binning scheme should be tuned to the specific application to get additional computational saving, and here, we investigate the optimal set for spectral binning and the number of EOFs in the Hartley and Huggins ozone bands (265-360 nm).

Optical properties within each bin must be strongly correlated to reduce the number of EOFs required to attain a given accuracy. According to Kopparla et al. (2016), the UV region is divided at 340 nm, beyond which O_2-O_2 absorption must be considered. In our application, the spectral region 340-360 nm is further divided at 350 nm: in the first sub-window, ozone absorption is much stronger than O_2-O_2, while for the second (350-360 nm), O_2-O_2 absorption becomes dominant. The binning criteria are generally determined by similarities in total optical depth of gas absorption profiles τ_{ij} as defined below:

$$\Gamma_g = -\ln \sum_{n=1}^{N_L} \sum_{j=1}^{N_g} \tau_{nj} , \qquad (9)$$

where N_L and N_g denote the number of atmospheric layers and atmospheric trace gases.

To evaluate the performance of the PCA approximation, the "exact-RT" model is executed in order to calculate a fully accurate multiple-scattering spectrum using the FO model for an accurate single scattering field and VLIDORT model for an accurate multiple scattering field:

$$I_{exact}(\lambda_i) = I_{VLD}(\lambda_i) + I_{FO}(\lambda_i). \qquad (10)$$

We first evaluate the impact of applying different binning steps and numbers of EOFs in Fig. 4. where the residuals $(I_{PCA} - I_{EXACT})$ are plotted as a function of Γ_g for the spectral window 265-340 nm at small and large SZAs, respectively. In this evaluation, the bins are equally spaced in Γ_g for the five steps from 0.20 to 1.0. For $\Gamma_g < 1$, where the extinction is strong enough that radiances are very small, the residuals are effectively reduced by having more bins rather than increasing the number of EOFs. In this optical range, using the first EOF is enough to capture the vast majority of the spectral variance, with the optimization of the binning step. However, the bins should be narrowly spaced with Γ_g intervals of at least 0.3-0.4 for those spectral grids for which Γ_g is less than -2. These spectral grids are correlated with the Hartley band above ~300 nm, where radiance values rapidly increase due to decreasing ozone absorption, but the spectral variations are almost unstructured. The rest of our spectral region corresponds to the Huggins band above 310 nm, where spectral variations are distinctly influenced by local maxima and minima of ozone absorption. In this spectral region, PCA approximation errors can be greatly reduced by increasing the number of EOFs. However, it is interesting to note that the PCA approximation is not further improved by using 4 EOFs instead of 3 (not shown here). Figure 4 also illustrates the dependence of the PCA performance on SZA in the spectral range below 340 nm: For example, when 2 EOFs are applied with the binning step 0.4, errors are within $\pm$ 0.02 % at smaller SZA, but increase up to $\pm$0.03 % at larger SZA. Therefore, as listed in Table 1, two sets of binning criteria are determined to keep the accuracy within 0.05 % for any

https://doi.org/10.5194/amt-2020-349
Preprint. Discussion started: 18 September 2020

viewing geometry. Based on the experiments shown in Fig. 5, the binning criteria are determined for the other sub-windows listed in Table 1, namely 340-350 nm and 350-360 nm: The former is set with bins at intervals of 1 and using the first two EOFs, while the latter is divided into a single bin with the first four EOFs. Figure 6 illustrates the binning criteria thus determined, demonstrating that the PCA performance keeps accuracies within 0.03 % when various sets of SZAs, ozone profiles, and vertical layers are implemented.

3.2 LUT-based correction

Two sets of LUTs are created, for high accuracy (LUT_H: vector/12 streams/72 layers), and low accuracy (LUT_L: scalar/4 streams/24 layers) configurations. The on-line PCA-VLIDORT model is configured to run in the "LUT_L" mode. The correction spectrum is straightforwardly calculated as the ratio of the LUT-based spectrum (LUT_H/LUT_L), but the radiance correction term is additionally adjusted to account for the different gas optical depth profiles used in on-line and LUT simulations. The RT results are corrected as follows.

$$I_{on} = I_{on,L} \times \exp\left(\ln(I_{LUT_H}/I_{LUT_L}) + \sum_{n=1}^{N_L} \left[\left(\frac{\partial \ln I}{\partial \tau}_{LUT_H} - \frac{\partial \ln I}{\partial \tau}_{LUT_L} \right) \times (\tau_{on} - \tau_{LUT}) \right](n) \right); \quad (11a)$$

$$\frac{\partial I}{\partial A_{s_{on}}} = \frac{\partial I}{\partial A_{s_{on,L}}} \times \frac{\frac{\partial I}{\partial A_{s_{LUT_H}}}}{\frac{\partial I}{\partial A_{s_{LUT_L}}}}; \qquad (11b)$$

$$\frac{\partial I}{\partial \tau_{on}} = \frac{\partial I}{\partial \tau_{on,L}} \times \frac{\partial I}{\partial \tau_{LUT_H}} / \frac{\partial I}{\partial \tau_{LUT_L}}, \qquad (11c)$$

where A_s and τ_n represent the surface albedos and gas absorption optical depths (n is the layer index). To construct LUTs, RT calculations are performed using the VLIDORT version 2.8 model for sets of geometrical configurations (θ, θ_o; solar zenith angle, viewing zenith angle), surface pressures for 22 climatological ozone profiles and 92 wavelengths (265-345 nm) as listed in Table 2. The azimuth dependence is treated exactly using the 0-2 Fourier intensity components in a Rayleigh scattering atmosphere in conjunction with the associated cosine-azimuth expansion of the full intensity; see the

Atmospheric Measurement Techniques Discussions

discussion below. The 22 ozone profiles are constructed from the GOME ozone profile product (Liu et al. 2005), where the ozone profile shapes vary according to three latitude regimes and with the total column ozone amounts at 50 DU intervals. The 92 wavelengths are regularly sampled at 5 nm intervals below 295 nm and at 1.0 nm intervals up to 310 nm in the Hartley band, while irregularly sampled based on the local minima and maxima of the ozone absorption structures in the Huggins band. The results of these RT calculations are separated into two components: the path radiance I_{atm} and the surface reflectance term I_{sfc} according to Chandrasekhar (1960), so that the following relationship is employed to recover the full radiance:

$$I(\theta, \theta_o, \varphi - \varphi_o, A_s) = I_{atm}(\theta, \theta_o, \varphi - \varphi_o) + I_{sfc}(\theta, \theta_o, A_s). \quad (12)$$

I_{atm} represents the purely atmospheric contribution to the radiance in the presence of a dark surface (zero albedo), and in a Rayleigh scattering atmosphere, this is given as a Fourier expansion in the cosine of the relative azimuth angle.

$$I_{atm}(\theta, \theta_o, \varphi - \varphi_o) = I_o(\theta, \theta_o) + \cos(\varphi - \varphi_o)\, I_1(\theta, \theta_o) + \cos 2(\varphi - \varphi_o)\, I_2(\theta, \theta_o). \quad (13)$$

However, it is more convenient to write this in the form:

$$I_{atm} = I_o(\theta, \theta_o)\left(1 + \mathrm{aq}_1 \cos(\varphi - \varphi_o)\, Z_1(\theta, \theta_o) + \mathrm{aq}_2 \cos 2(\varphi - \varphi_o)\, Z_2(\theta, \theta_o)\right); \quad (14a)$$

$$Z_1(\theta, \theta_o) = \frac{1}{\mathrm{aq}_1} \frac{I_1(\theta, \theta_o)}{I_0(\theta, \theta_o)}; \qquad Z_2(\theta, \theta_o) = \frac{1}{\mathrm{aq}_2} \frac{I_2(\theta, \theta_o)}{I_0(\theta, \theta_o)}; \quad (14b)$$

$$\mathrm{aq}_1 = \frac{3}{8} \cos\theta \sin\theta\, sin\theta_o; \;\; \mathrm{aq}_2 = \frac{3}{32} \frac{(\sin\theta \;\; \sin\theta_o)^2}{cos\theta_o}. \quad (14c)$$

In the LUTs, the three coefficients (I_o, Z_1, and Z_2) are stored instead of I_{atm}. Note that the use of terms aq_1 and aq_2 is taken from Dave (1964); most of the angular variability in components I_1 and I_2 are captured analytically with these functions. In other words, Z_1 and Z_2 are angularly smooth and well-behaved (non-singular) functions, which helps improve angular interpolation accuracy with fewer points in the angular grids. The surface term is

$$I_{sfc}(\theta,\theta_o,A_s) = \frac{A_s T(\theta,\theta_o)}{1 - A_s s^*}. (15)$$

In the LUTs, we store the transmission term $T(\theta,\theta_o)$, which is the product of the atmosphere downwelling flux transmittance for a solar source with the upwelling transmittance from a surface illuminated isotropically from below, and the geometry-independent term s^* which is the spherical albedo from such a surface. This is the so-called "planetary problem" calculation (Chandrasekhar, 1960), and the code to obtain T and s^* is now implemented in VLIDORT Version 2.8 (Spurr, 2019). One of the key features of the VLIDORT code is its ability to generate simultaneously (along with the Stokes vector radiation field) any set of Jacobians with respect to atmospheric and surface optical properties. VLIDORT also contains an analytical linearization of the planetary problem. Indeed, in our Rayleigh-based application, we require Jacobians with respect to the albedo A_s and the ozone profile elements τ. First for the albedo weighting function we have straightforward differentiation from Equation (15) as following

$$\frac{\partial I}{\partial A_s} = T(\theta,\theta_o)\ \left(\frac{qr}{A_s}\right)^2; \qquad qr = A_s/(1 - A_s s^*). \quad (16)$$

For the optical depth derivative, $\partial I/\partial\tau$ is calculated from

$$\frac{\partial I}{\partial\tau} = \frac{\partial I_o}{\partial\tau} + \mathrm{aq}_1\cos(\varphi-\varphi_o)\frac{\partial Z_1}{\partial\tau} + \mathrm{aq}_2\cos 2(\varphi-\varphi_o)\frac{\partial Z_2}{\partial\tau} + qr.\frac{\partial T}{\partial\tau} + T.(\mathrm{qr})^2.\frac{\partial s^*}{\partial\tau}. (17)$$

All partial derivatives in this expression are returned automatically by VLIDORT. For a given ozone profile, wavelength, and surface pressure, the number of the LUT values specified in Table 3 is 770 ($\mathrm{nVar}\ \times\ \mathrm{n}\theta\ \times \mathrm{n}\theta_o + S_b + \frac{dS_b}{d\tau}$, $\mathrm{nVar} = 8$: I_o, $Z_1, Z_2, T, \frac{dI_o}{d\tau}, \frac{dZ_1}{d\tau}, \frac{dZ_2}{d\tau}, \frac{dT}{d\tau}$), which is much smaller than that of a LUT with dependence on 8 relative azimuth angles and 5 surface albedo values ($11{,}520 = \mathrm{nVar} \times \mathrm{n}\theta\ \times \mathrm{n}\theta_o \times \mathrm{n}(\varphi-\varphi_o) \times \mathrm{nA_s}$, $\mathrm{nVar} = 3: \mathrm{I}, \partial\mathrm{I}/\partial\tau, \partial\mathrm{I}/\partial\mathrm{A_s}$). LUT-based simulated radiances are evaluated against on-line simulations: The LUT interpolation errors

https://doi.org/10.5194/amt-2020-349
Preprint. Discussion started: 18 September 2020

are mostly less than 0.2-0.3 % (not shown here), except for extreme path length scenarios (e.g., ~1% at $\theta_o = 87.0°$) as shown in Fig. 7 a.b, However the interpolation errors are quite similar to each other for LUT_H and LUT_L. Therefore, those errors are canceled out when performing corrections using the two LUTs and thereby the overall error after LUT correction is much smaller than ~ 0.05 % (Fig. c). Note that the accuracy is completely maintained with respect to both $\varphi - \varphi_o$ and A_s, while the size of a LUT is reduced by a factor of 15. However, LUT corrections still contain ozone profile shape errors due to the use of 22 representative total ozone-dependent ozone profiles in the LUT. Figure 8 shows an example of the correction spectrum as a function of SZA, showing that polarization errors are mostly dominant, except at the high SZAs above 310 nm, where errors due to use of a low number of streams become significant, and for wavelengths below 300 nm where the use of the coarse vertical layering scheme becomes the main source of uncertainty.

4. **Evaluation**

The PCA-RT model developed as described in this paper is implemented as the forward model component of an iterative OE based inversion for retrieving ozone profile from OMI measurements. In previous studies, the PCA-RT performance was evaluated against a suite of exact monochromatic baseline of fully accurate VLIDORT simulations. However, such exact RT calculations cannot be applied in the operational data processing system, especially when thousands of spectral points are involved; in other words, the operational capability of the PCA-RT approach has been overestimated in previous studies. Therefore, we evaluate the RT model developed against the existing forward model where many RT approximations are applied to meet the computational budget in the operational system.

Table 4 contains sets of configurations for 7 forward models. OMI spectra are simulated at the under-sampled ("US") intervals specified in the first column of this table and then interpolated at high-resolution ("HR") intervals (second column) with the undersampling correction before convolution with OMI slit functions. In the v1 forward model, the US spectral intervals were set at 1.0 nm/0.4 nm intervals below/above 295 nm and 0.6 nm above 310 nm, while the HR spectral interval was set at 0.05 nm. In the updated RT model, the spectral points are selected at 0.3 nm (0.1 nm) intervals below (above) 305 nm and the HR interval is set as 0.03 nm, which enables us to achieve very high-accuracy, better than 0.01 %, as shown in Fig. 2.c. In the reference configuration (abbreviated to "Ref"), VLIDORT is run in vector mode with 12 streams and 72 atmospheric layers, so that the RT approximation errors are

https://doi.org/10.5194/amt-2020-349
Preprint. Discussion started: 18 September 2020

Atmospheric Measurement Techniques Discussions

significantly eliminated. The VLIDORT-based forward model is run with five sets of configurations (abbreviated to "VLD" in Table 4) to quantify the impact of RT approximations on ozone retrievals. Figure 10 compares the mean biases of the retrieved ozone profiles between VLD/PCA and Ref for three SZA regimes. VLD^0 represents the v1 forward model configuration, demonstrating that the ozone retrieval errors due to the entire forward model errors range from ~ 2 % for the large SZA regime to ~ 5 % for the small SZA regime at the lower atmospheric layers, but ~ 1 % at the upper layers. The configuration VLD^1 assesses the impact of undersampling errors on the retrievals, causing negative biases of up to 2.0 % below ~ 20 km. Compared to the use of 12 streams, using 8 streams causes negligible impacts on ozone retrievals (VLD^2) as the corresponding RTM approximation errors are negligible, except for extreme viewing geometries where the ozone retrieval errors are overwhelmed by instrumental measurement errors (a few %), rather than the forward model errors of ~ 0.05 % as shown in Fig. 3. The VLD^3 based RT calculation is applied to ozone retrievals for evaluating on-line polarization correction, showing that the corresponding errors in tropospheric ozone retrievals are estimated as ± 2 % at small SZAs. The evaluation for VLD^4 demonstrates that the use of coarse atmospheric layering causes the largest errors (~4.5 % in the troposphere, ~ 1.5 % in the stratosphere). PCA^o represents the v2 forward model configuration while PCA^1 is done in the highest accurate configuration except for PCA approximation. Retrieval errors due to PCA approximation are negligible except for the bottom few layers at smaller solar zenith angles (up to ~ 1.5 %). Differences between PCA^o and PCA^1 represents the ozone retrieval errors due to LUT errors, mostly related to the profile shape errors between LUT and on-line calculations. In Fig. 10, the comparison between VLD0 (v1 PROFOZ) and PCA0 (v2 PROFOZ) is performed for individual ozone profile retrievals. The large systematic errors of ~ 5- 15 % due to v1 forward model errors are greatly eliminated below 30 km. In addition, the random-noise errors are significantly eliminated over the entire layers at high solar zenith angles. However, there are still some remaining retrieval errors up to - 5% in troposphere and 3 % in stratosphere due to v2 forward model simulation errors. Figure 11 further evaluates the v2 implementation. First of all, the comparison of the runtime (Fig 11.a) demonstrates a 3.3-fold-increase in speed on average, thanks to switching the forward model from v1 to v2. Some spectral fit residuals are eliminated in the UV 1 band over the middle area of the swath (low latitudes), where the SZAs are relatively small, by up to ~ 2 %; the corresponding improvements are found in the stratospheric column ozone. The amount of the stratospheric column ozone deviated from the reference is reduced by ~ 0.2 % with v2 implementation. On the other hand, the tropospheric column ozone retrievals show improvements for most cases, whereas the fit residuals of the UV2 band are slightly worse in the low latitudes, but significantly better (2-5 %) in the Northern high latitudes (OMI along-track number > ~

https://doi.org/10.5194/amt-2020-349
Preprint. Discussion started: 18 September 2020

Atmospheric Measurement Techniques Discussions

1300).

5. Summary and Conclusions

We have extended the PCA-based fast RT method to overcome computational challenges for OE-based SAO OMI ozone profile retrievals from ultraviolet measurements requiring iterative calculations of the radiance and its Jacobian derivatives, to match the simulated spectrum to the measured spectrum The PCA-RT model is designed to perform MS calculations for a few EOF-derived optical states which are developed from spectrally binned sets of inherent optical properties that possess some redundancy. To maximize the performance enhancement, we carefully tuned the binning scheme for the UV ozone fitting window from 265 nm to 360 nm in such a way as to choose the number of EOFs to be as small as possible for each bin, rather than always using the first four EOFs for all bins selected in previous studies. The spectral windows are divided into three sub-windows: 1) 265-340 nm, 2) 340-350, and 3) 350-360 nm. Then, optical profiles are grouped into bins according to criteria based on the total gas optical depth, as specified in Table 1. Spectral bins correlated to the Hartley ozone band use only the first EOF, but 2 or 3 EOFs are required for those bins related to the Huggins ozone band. The MS model is executed 85 times for the entire wavelength range (265-360 nm), and only 51 times for the OMI ozone fitting window (270-330 nm). We demonstrated that the PCA approximation errors are within 0.03 % for any viewing geometry, optical depth profile, and vertical layering. The existing (v1) forward model calculations are evaluated to determine the optimal configuration for the v2 forward model. RT approximation errors exist due to the use of 24 quite coarse vertical layers (2.5 km thick), which can cause radiance simulation errors of up to ~ 1 % below 320 nm and this leads to ozone retrieval errors of 2-4 % in the troposphere and 1 % in the stratosphere. Eight-stream calculations can result in radiance residuals of ~ 0.05 % or less except at extreme viewing geometries, which causes trivial errors on ozone retrievals compared to other error factors. In spite of accounting for polarization errors using vector and scalar differences at 14 wavelengths, the retrieval accuracies are systematically worse by ~ 2 % due to neglecting second-order polarization errors which are strongly correlated with ozone absorption features. We found that 72 atmospheric layers (~ 0.7 km thick) and 12 streams should be used at least for fully accurate RT calculations comparable to those with 99 atmospheric layers and 32 streams. The OMI spectral fit uses 229 wavelengths at OMI native grids, but the existing RT model simulates 93 wavelengths and is then interpolated onto 0.05 nm grids with undersampling correction. However, we found room to improve our retrievals (~ 1.5 % on avearge) by simulating 244 wavelength grids selected at intervals of 0.3 nm/0.1 nm below/above 305 nm and then performing the undersampling correction to 0.03 nm. Applying the PCA-RT approach allows us to reduce the number of MS calculations from the high-resolution optical dataset to 51

https://doi.org/10.5194/amt-2020-349
Preprint. Discussion started: 18 September 2020

Atmospheric Measurement Techniques Discussions

sets of EOF-derived optical states, but the performance savings are not enough to improve over previous RT approximations. To improve both efficiency and accuracy, we have developed a LUT-based correction for eliminating the RT approximation errors arising from the vector vs scalar, 12 vs. 4 streams, and 72 vs. 24 layers. In conclusion, the updated PCA-based RT model combined with LUT corrections makes ozone profile retrievals faster than the v1 forward model by a factor of 3.3 on average. Improvements in fitting accuracies are also achieved in the UV1 band by 2 % and in the UV2 band by 2-5 %. Correspondingly, the ozone profile retrievals are significantly improved, especially in the troposphere by ~ up to 10 %. However, there are still some remaining retrieval errors of up to - 5% in troposphere and 3 % in stratosphere due to the LUT correction errors and PCA approximation errors in the v2 implementation. The updated forward model is in preparation for reprocessing all OMI measurements (2004 -current) for the next version of the PROFOZ product.

Author contributions. JB and XL designed the research; RS provided oversight and guidance for using both VLIDORT and PCA-based VLIDORT; KY developed the LUT creation and interpolation scheme; XL contributed to analyzing ozone profile retrievals with different forward model approaches; JB conducted the research and wrote the paper; CN, CM, GA, and KC contributed to the analysis and writing; CM and GA contributed to managing the computational resources.

Competing interests. The authors declare that they have no conflicts of interest.

Data availability. OMI Level1b radiance datasets are available at https://aura.gesdisc.eosdis.nasa.gov/data/Aura_OMI_Level1/ (last access: 31 AUG 2020). The LUT database are attainable upon request.

Acknowledgments We acknowledge the OMI science team for providing their satellite data. Research at the Smithsonian Astrophysical Observatory is funded by the NASA Aura science team program (NNX17AI82G). Research at Pusan National University is funded by Basic Science Research Program through the National Research Foundation of Korea(NRF) funded by the Ministry of Education(2020R1A6A1A03044834).

Financial support. This research has been supported by NASA Aura science team program (grant no. NNX17AI82G) and Basic Science Research Program through the National Research Foundation of Korea(NRF) funded by the Ministry of Education(2020R1A6A1A03044834).

https://doi.org/10.5194/amt-2020-349
Preprint. Discussion started: 18 September 2020

Atmospheric Measurement Techniques Discussions

References

Chandrasekhar, S.: Radiative Transfer, Dover Publications, Mineola, New York, 1960.

Cuesta, J., Eremenko, M., Liu, X., Dufour, G., Cai, Z., Höpfner, M., von Clarmann, T., Sellitto, P., Foret, G., Gaubert, B., Beekmann, M., Orphal, J., Chance, K., Spurr, R., and Flaud, J.-M.: Satellite observation of lowermost tropospheric ozone by multispectral synergism of IASI thermal infrared and GOME-2 ultraviolet measurements over Europe, Atmos. Chem. Phys., 13, 9675–9693, https://doi.org/10.5194/acp-13-9675-2013, 2013.

Dave, J.V.: Meaning of Successive Iteration of the Auxiliary Equation in the Theory of Radiative Transfer, The Astrophysical Journal, 140, 1292-1303, 1964.

Efremenko D. S., Loyola, D. G., Spurr, R., and Doicu, A.: Acceleration of Radiative Transfer Model Calculations for the Retrieval of Trace Gases under Cloudy Conditions. J. Quant. Spectrosc. Radiat. Transfer., 135, 58-65, 2014.

Fu, D., Kulawik, S. S., Miyazaki, K., Bowman, K. W., Worden, J. R., Eldering, A., Livesey, N. J., Teixeira, J., Irion, F. W., Herman, R. L., Osterman, G. B., Liu, X., Levelt, P. F., Thompson, A. M., and Luo, M.: Retrievals of tropospheric ozone profiles from the synergism of AIRS and OMI: methodology and validation, Atmos. Meas. Tech., 11, 5587-5605, https://doi.org/10.5194/amt-11-5587-2018, 2018.

Fu, D., Worden, J. R., Liu, X., Kulawik, S. S., Bowman, K. W., and Natraj, V.: Characterization of ozone profiles derived from Aura TES and OMI radiances, Atmos. Chem. Phys., 13, 3445-3462, https://doi.org/10.5194/acp-13-3445-2013, 2013.

Kim, P. S., Jacob, D. J., Liu, X.,Warner, J. X., Yang, K., Chance, K., Thouret, V., and Nedelec, P.: Global ozone–CO correlations from OMI and AIRS: constraints on tropospheric ozone sources, Atmos. Chem. Phys., 13, 9321–9335, https://doi.org/10.5194/acp-13-9321-2013, 2013.

Kopparla, P., Natraj, V., Limpasuvan, D., Spurr, R., Crisp, D., Shia, R.L., Somkuti, P., Yung, Y.L.; PCA-based radiative transfer: Improvements to aerosol scheme, vertical layering and spectral binning. *J. Quant. Spectrosc. Radiat. Transf., 198*, 104–111, 2017.

Kopparla, P., Natraj, V., Spurr, R., Shia, R.L., Crisp, D., Yung, Y.L.; A fast and accurate PCA based radiative transfer model: Extension to the broadband shortwave region. *J. Quant. Spectrosc. Radiat. Transf., 173*, 65–71, 2016.

Kroon, M., Petropavlovskikh, I., Shetter, R., Hall, S., Ullmann, K., Veefkind, J. P., McPeters, R. D., Browell, E. V., and Levelt, P. F.: OMI total ozone column validation with Aura-AVE CAFS observations, J. Geophys. Res., 113, D15S13, doi:10.1029/2007JD008795, 2008.

Liu, C., Yao, B., Natraj. V., Kopparla, P., Weng., F., Le., T., Shia., R.., and Yung, Y. L.: A spectral Data Compression (SDCOMP) Radiative Transfer Model for High-Spectral-Resolution Radiation Simulations, J. Atmos., Sci., 77, 2055-2066, https://doi.org/10.1175/JAS-D-19-0238.1, 2020.

Liu, X., Bhartia, P.K, Chance, K, Spurr, R.J.D., and Kurosu, T.P.: Ozone profile retrievals from the ozone monitoring instrument. Atmos. Chem. Phys., 10, 2521–2537, 2010.

Liu, X., Yang, Q., Li, H., Jin, Z., Wu, W., Kizer, S., Zhou., D. K., and Yang., P.; Development of a fast and accurate pcrtm radiative transfer model in the solar spectral region. Applied optics, 55(29), 8236–8247., 2016.

Loyola, D. G., Gimeno García, S., Lutz, R., Argyrouli, A., Romahn, F., Spurr, R. J. D., Pedergnana, M., Doicu, A., Molina García, V., and Schüssler, O.: The operational cloud retrieval algorithms from TROPOMI on board Sentinel-5 Precursor, Atmos. Meas. Tech., 11, 409–427, https://doi.org/10.5194/amt-11-409-2018, 2018.

Miles, G. M., Siddans, R., Kerridge, B. J., Latter, B. G., and Richards, N. A. D.: Tropospheric ozone and ozone profiles retrieved from GOME-2 and their validation, Atmos. Meas. Tech., 8, 385–398,

https://doi.org/10.5194/amt-2020-349
Preprint. Discussion started: 18 September 2020

Atmospheric Measurement Techniques Discussions

https://doi.org/10.5194/amt-8-385-2015, 2015.

Nanda, S., de Graaf, M., Veefkind, J. P., ter Linden, M., Sneep, M., de Haan, J., and Levelt, P. F.: A neural network radiative transfer model approach applied to the Tropospheric Monitoring Instrument aerosol height algorithm, Atmos. Meas. Tech., 12, 6619–6634, https://doi.org/10.5194/amt-12-6619-2019, 2019.

Natraj, V., Jiang, X., Shia, R.-L., Huang, X., Margolis, J. S., and Yung, Y. L.; Application of principal component analysis to high spectral resolution radiative transfer: A case study of the O_2-A band, *J. Quant. Spectrosc. Radiat. Transf.*, 95(4), 539–556. https://doi.org/10.1016/j.jqsrt.2004.12.024, 2005.

Natraj, V., Shia, R. L., and Yung, Y. L.;. On the use of principal component analysis to speed up radiative transfer calculations, *J. Quant. Spectrosc. Radiat. Transf.*, 111(5), 810–816. https://doi.org/10.1016/j.jqsrt.2009.11.004, 2010.

Somkuti, P., Boesch, H., Vijay, N., and Kopparla, P.; Application of a PCA-based fast radiative transfer model to XCO2 retrievals in the shortwave infrared, *J. Geophys. Res*: Atmospheres, 122, 10,477–10,496. https://doi.org/10.1002/2017JD027013., 2017.

Rodgers, C. D.; Inverse methods for atmospheric sounding—Theory and practice. In C. D. Rodgers (Ed.), Series on atmospheric oceanic and planetary physics (Vol. 2). Oxford: World Scientific Publishing Co. Pte. Ltd. https://doi.org/10.1142/9789812813718, 2000.

Spurr, R., Natraj, V., Lerot, C., Van Roozendael, M., and Loyola, D.; Linearization of the principal component analysis method for radiative transfer acceleration: Application to retrieval algorithms and sensitivity studies, *J. Quant. Spectrosc. Radiat. Transf.*, 125, 1–17. https://doi.org/10.1016/j.jqsrt.2013.04.002, 2013.

Spurr, R., Natraj, V., Kopparla, P., and Christi, M.; Application of Principal Component Analysis (PCA) to Performance Enhancement of Hyperspectral Radiative Transfer Computations, in "Principal Component Analysis: Methods, Applications and Technology", NOVA publishers, 2016

Spurr, R.; User's Guide VLIDORT version 2.8.1, RT Solutions, Inc., 9 Channing Street, Cambridge, MA 02138, USA., 2019.

Spurr, R. and Christi, M. : The LIDORT and VLIDORT Linearized Scalar and Vector Discrete Ordinate Radiative Transfer Models: An Update for the last 10 Years. Light Scattering Reviews, Volume 12, ed. A. Kokhanovsky, Springer, 2019.

Yang, Q., Liu, X., Wu, W., Kizer, S., and Baize, R. R.: Fast and accurate hybrid stream PCRT M-SOLAR radiative transfer model for reflected solar spectrum simulation in the cloudy atm osphere, Opt. Express **24**, A1514-A1527, 2016.

Zoogman, P., Liu, X., Suleiman, R. M., Pennington, W. F., Flittner, D. E., Al-Saadi, J. A., Hilton, B. B., Nicks, D. K., Newchurch, M. J., Carr, J. L., Janz, S. J., Andraschko, M. R., Arola, A., Baker, B. D., Canova, B. P., Chan Miller, C., Cohen, R. C., Davis, J. E., Dussault, M. E., Edwards, D. P., Fishman, J., Ghulam, A., González Abad, G., Grutter, M., Herman, J. R., Houck, J., Jacob, D. J., Joiner, J., Kerridge, B. J., Kim, J., Krotkov, N. A., Lamsal, L., Li, C., Lindfors, A., Martin, R. V., McElroy, C. T., McLinden, C., Natraj, V., Neil, D. O., Nowlan, C. R., O'Sullivan, E. J., Palmer, P. I., Pierce, R. B., Pippin, M. R., Saiz-Lopez, A., Spurr, R. J. D., Szykman, J. J., Torres, O., Veefkindz, J. P., Veihelmann, B.,Wang, H.,Wang, J., and Chance, K.: Tropospheric Emissions: Monitoring of Pollution (TEMPO), *J. Quant. Spectrosc. Radiat. Transf.*, 186, 17–39, https://doi.org/10.1016/j.jqsrt.2016.05.008, 2017.

https://doi.org/10.5194/amt-2020-349
Preprint. Discussion started: 18 September 2020

Atmospheric Measurement Techniques Discussions

Table 1. The PCA-RT configuration optimized over the UV spectral range 265-360 nm. The optical depth of the total gas column (Γ_g defined in eq. 9) is used to set the criteria for the spectral binning; for example, one or more bins are created at intervals ($\Delta\Gamma_g$) in the range Γ_g^{min} to Γ_g^{max}. For each bin, the optical states are expanded in terms of the first few number of EOFs (nEOF).

265-340 nm							
SZA or VZA < 70°				SZA or VZA ≥ 70°			
List	Γ_g^{lower}, Γ_g^{upper}	$\Delta\Gamma_g$	nEOF	List	Γ_g^{lower}, Γ_g^{upper}	$\Delta\Gamma_g$	nEOF
1	∞ to -1.7	2	1	1	∞ to - 1.5	2.0	1
2	-1.7 to -1.2	0.5	1	2	-1.5 to -0.7	1.2	1
3	-1.2 to 0.0	0.4	1	3	-0.7 to 0.4	0.35	1
4	0.0 to 0.5	0.5	1	4	0.4 to 0.7	0.3	1
5	0.5 to 3.5	0.6	2	5	0.7 to 2.5	0.6	3
6	3.5 to 4.5	1.0	2	6	2.5 to 3.5	1.0	3
7	4.5 to ∞	2.0	2	7	3.5 to 4.5	1.0	2
8				8	4.5 to ∞	2.0	2
340-350 nm				350-360 nm			
List	Γ_g^{lower}, Γ_g^{upper}	$\Delta\Gamma_g$	nEOF	List	Γ_g^{lower}, Γ_g^{upper}	$\Delta\Gamma_g$	nEOF
1	∞ to ∞	1.0	2	1	∞ to ∞	∞	4

Table 2. LUT parameter specification. Note that the relative azimuth dependence is taken into account explicitly through the Fourier coefficients of path radiance (Table 3) and the surface albedo dependence is taken into account by the planetary problem.

Parameter	Symbol	N	Grid Values
Ozone Profile[+]	O_3P	22	• Low-latitude (30°S-30°N) L200,L250,L300,L350 • Mid-latitude (30°-60°N/S) M200,M250,M300,M350, M400,M450, M500,M550 • High-latitude (60°-90°N/S) H100,H150,H200,H250,H300,H350, H400,H450, H500,H550
Wavelength	λ	92	265-345 nm
Solar Zenith Angle	θ_o,	12	0, 16, 31, 44, 55, 64, 71, 76.5, 80.5, 83.5, 86, 88°
Viewing Zenith Angle	θ	8	0, 15, 30, 43, 53, 61, 67, 72°
Surface albedo	A_s	1	0.0
Surface pressure	P_s	12	100, 150, 200, 300, 400, 500, 600, 700, 800, 900, 1013.25, 1050 hPa

[+]Total ozone-based ozone profiles for three latitude regimes. The grid values represent the

https://doi.org/10.5194/amt-2020-349
Preprint. Discussion started: 18 September 2020

Atmospheric Measurement Techniques Discussions

amount of total ozone (DU).

Table 3. LUT variable specification

Variable	Dimensions	Variable	Dimensions
$\boldsymbol{I_o}$[a]	$n\lambda, n\theta, n\theta_o, nP_s$	$dI_o/d\tau$	$n\lambda, n\theta, n\theta_o, nz, nP_s$
$\boldsymbol{Z_1}$[a]	$n\lambda, n\theta, n\theta_o, nP_s$	$dZ_1 d\tau$	$n\lambda, n\theta, n\theta_o, nz, nP_s$
$\boldsymbol{Z_2}$[a]	$n\lambda, n\theta, n\theta_o, nP_s$	$dZ_2/d\tau$	$n\lambda, n\theta, n\theta_o, nz, nP_s$
$\boldsymbol{T}$[b]	$n\lambda, n\theta, n\theta_o, nP_s$	$dT/d\tau$	$n\lambda, n\theta, n\theta_o, nz, nP_s$
$\boldsymbol{S_b}$[c]	$n\lambda, nP_s$	$dS_b/d\tau$	$n\lambda, nz, nP_s$
$\boldsymbol{\tau}$[d]	$n\lambda, nz^+$		

[a] Fourier coefficients of path radiance with respect to relative azimuth angle
[b] total transmission of the atmosphere
[c] spherical albedo of the atmosphere
[d] total gas absorption optical depth profile
[+] Number of atmospheric layers

Table 4. List of configurations used in evaluating the different forward model calculations for OMI ozone profile retrievals. The reference, VLIDORT, and PCA-RT models are abbreviated as Ref, VLD, and PCA, respectively.

RT models	US SI (nm) [a]	HR SI (nm) [b]	Nstream[c]	Nlayer[d]	Polarization[e]	RT corr[f]
Ref	0.3(<305nm) 0.1 (≥305 nm)	0.03	12	72	True	False
VLD^o	1.0(<295nm) 0.4(between) 0.6 (≥310 nm)	0.05	8	24	False	On-line polcorr
VLD^1	1.0(<295nm) 0.4(between) 0.6 (≥310 nm)	0.05	12	72	True	False
VLD^2	0.3(<305nm) 0.1 (≥305 nm)	0.03	8	72	True	False
VLD^3	0.3(<305nm) 0.1 (≥305 nm)	0.03	12	72	False	On-line polcorr
VLD^4	0.3(<305nm) 0.1 (≥305 nm)	0.03	12	24	True	False
PCA^0	0.3(<305nm) 0.1 (≥305 nm)	0.03	4	24	False	LUT
PCA^1	0.3(<305nm) 0.1 (≥305 nm)	0.03	12	72	True	False

[a] Under-sampled (US) spectral intervals (nm) used to define wavelengths at which RT is actually executed.
[b] High-resolution (HR) spectral intervals (nm) used to define wavelengths where under-sampled simulations are interpolated before spectral convolution.

https://doi.org/10.5194/amt-2020-349
Preprint. Discussion started: 18 September 2020

Atmospheric Measurement Techniques
Discussions

[c] the number of discrete ordinates in the full polar space; [d]Number of atmospheric layers
[e]RT model is run in the vector (scalar) mode if polarization is true (false).
[f]On-line polarization correction as described in Section 2, which is originally developed from Liu et al. (2010). LUT-based correction introduced in Section 3.3, which is developed in this work to account for RT approximation errors due to neglecting polarization as well as using 4 streams and 24 layers.

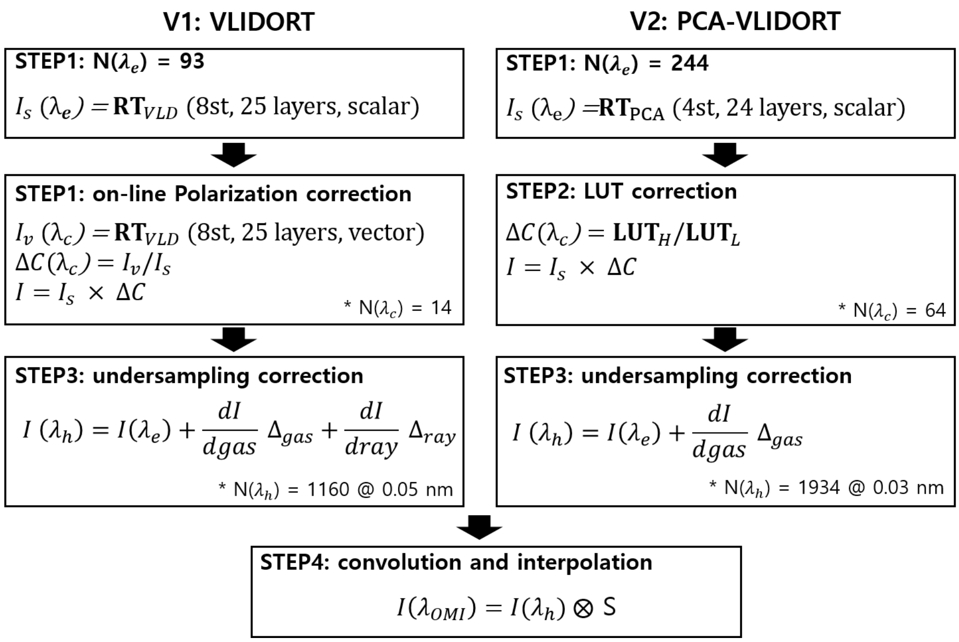

Fig.1. Schematic flowcharts of VLIDORT (v1) and PCA-VLIDORT (v2) based forward models, respectively. Note that VLIDORT was used in the generation of the OMPROFOZ v1 dataset, while PCA-VLIDORT is in preparation for OMPROFOZ v2 production. The number of wavelengths used in each process is denoted as $N(\lambda)$ when the spectral window 270-330 nm is applied. λ_e represents the wavelength grids used for RT calcluation, while λ_c and λ_h are grids used in RT approximation correction and undersampling correction, respectively. See text for definition of other variables.

https://doi.org/10.5194/amt-2020-349
Preprint. Discussion started: 18 September 2020

Atmospheric Measurement Techniques
Discussions

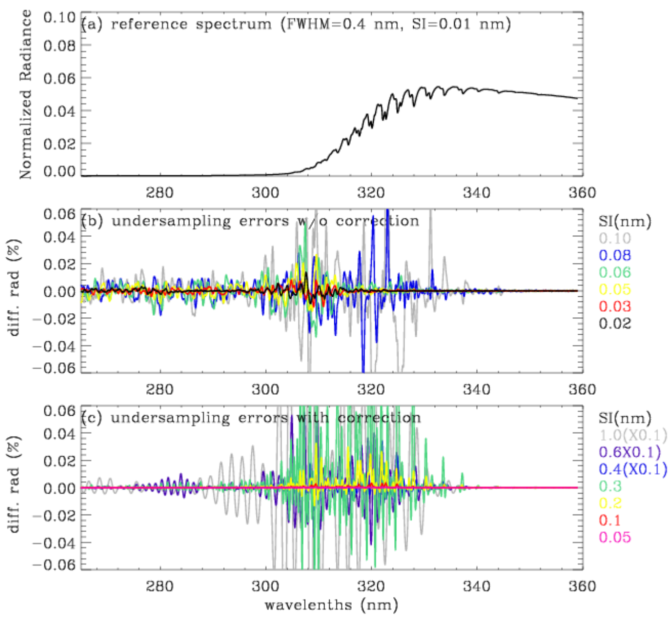

Fig.2. (a) Reference (truth) normalized radiance spectrum simulated at the spectral intervals (SIs) of 0.01 nm in 265-360 nm (solar zenith angle = 65 º, viewing zenith angle = 30 º, relative azimuth angle = 120º), which is used for evaluating the simulations in Figs. (b) and (c). (b) Impact of under-sampling on the simulation. (c) is similar to (b), but now the under-sampling correction has been applied. In Fig 2(c), the under-sampling errors are divided by 10 at SIs ≥ 0.4 nm. Note that individual radiances simulated at different SIs are interpolated to 0.01 nm and then convolved with the Gaussian function (FWHM: 0.4 nm) which represents the OMI instrument spectral response function.

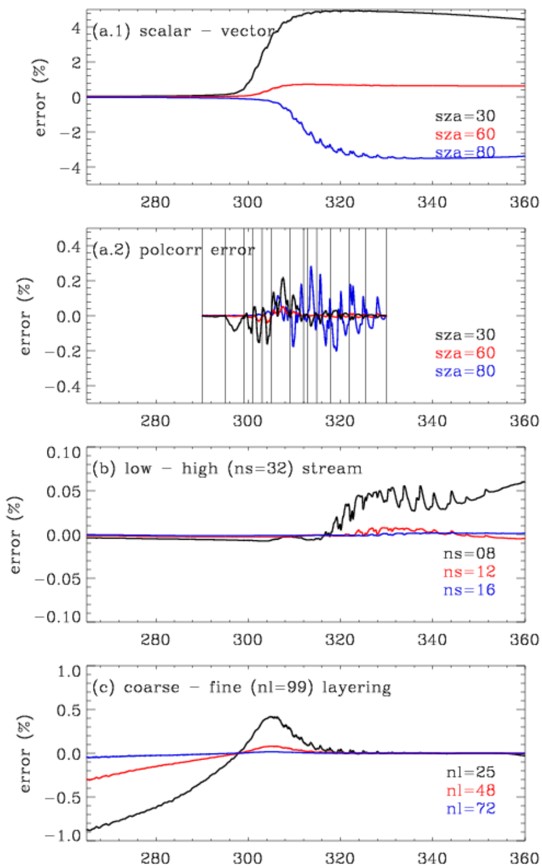

Fig. 3. Errors of the radiance simulation due to the RT approximation used in v1, arising from (a.1) neglecting the polarization effect for different solar zenith angles (sza), (a.2) polarization correction errors, (b) using a low number of streams (ns), and (c) using a coarse number of vertical grids (nl). Note that vertical lines in Fig. 3.a.2 indicate wavelengths used in deriving the on-line polarization correction spectrum.

https://doi.org/10.5194/amt-2020-349
Preprint. Discussion started: 18 September 2020

Atmospheric Measurement Techniques
Discussions

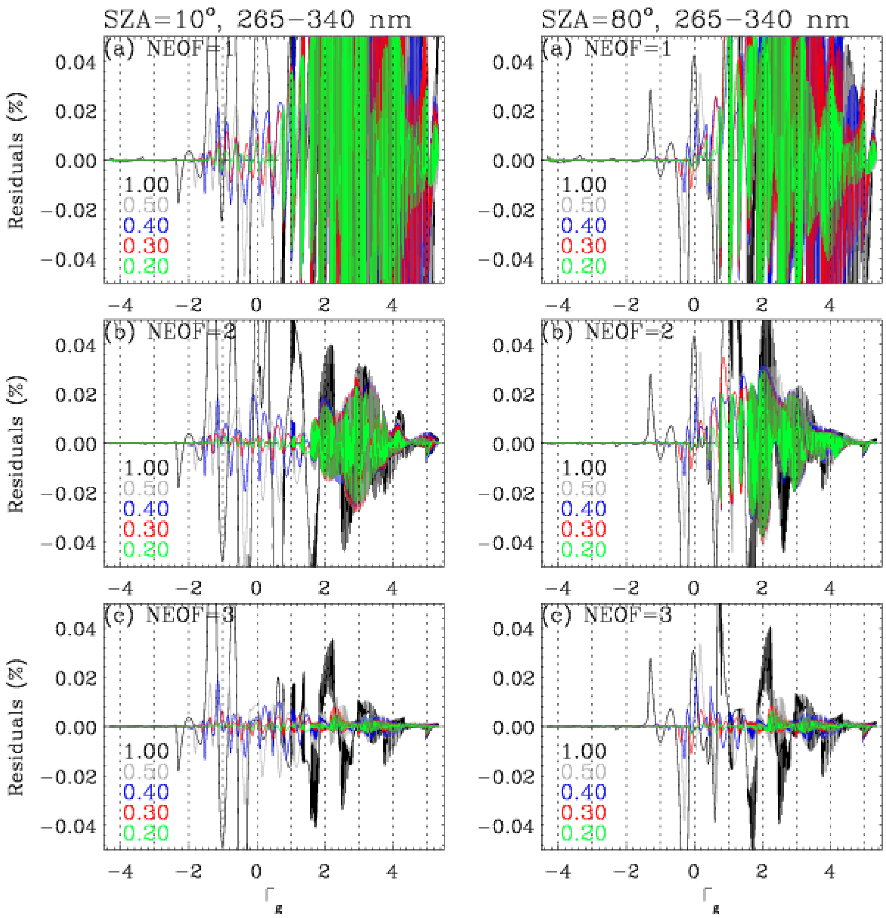

Fig. 4. Residuals (%) of the PCA-RT radiance in the wavelength range 265-340 nm compared to the exact-RT calculations, for different binning steps (different colors) and number of EOFs (a, b, c). Results are plotted as a function of Γ_g (logarithm of the total gas optical depth), for solar zenith angles (SZAs) of (left)10° and (right) 80°.

https://doi.org/10.5194/amt-2020-349
Preprint. Discussion started: 18 September 2020

Atmospheric Measurement Techniques
Discussions

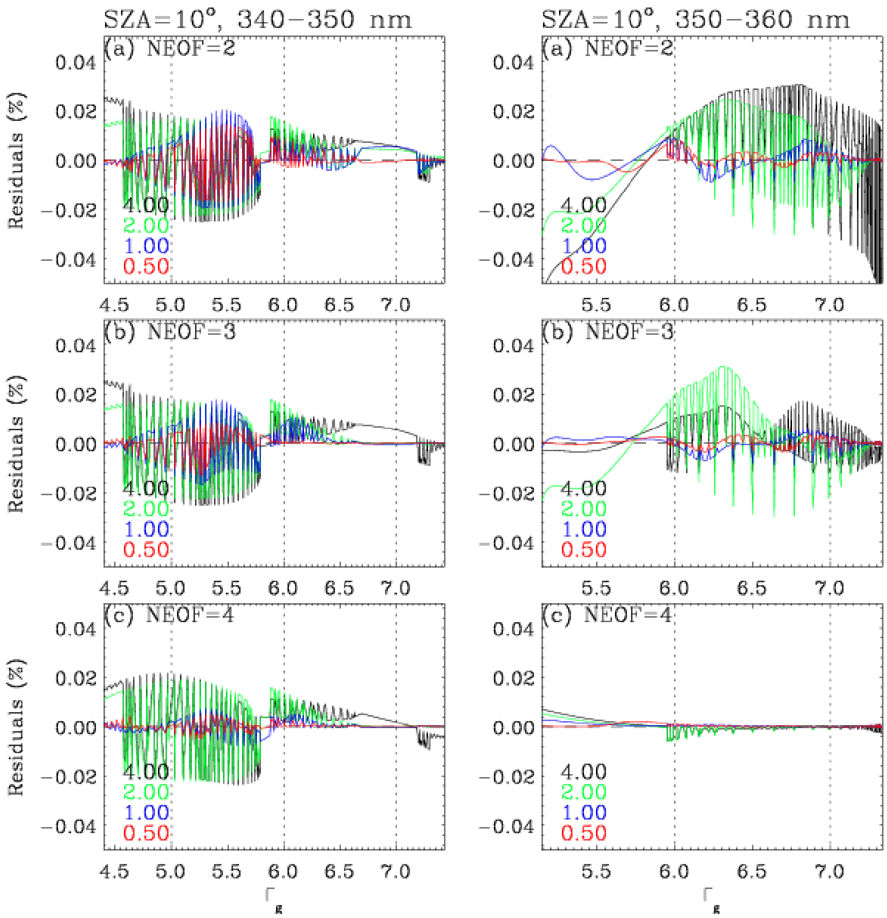

Fig. 5. Same as Fig. 4, but for different windows, (left) 340-350 nm and (right) 350-360 nm, respectively.

https://doi.org/10.5194/amt-2020-349
Preprint. Discussion started: 18 September 2020

Atmospheric Measurement Techniques
Discussions

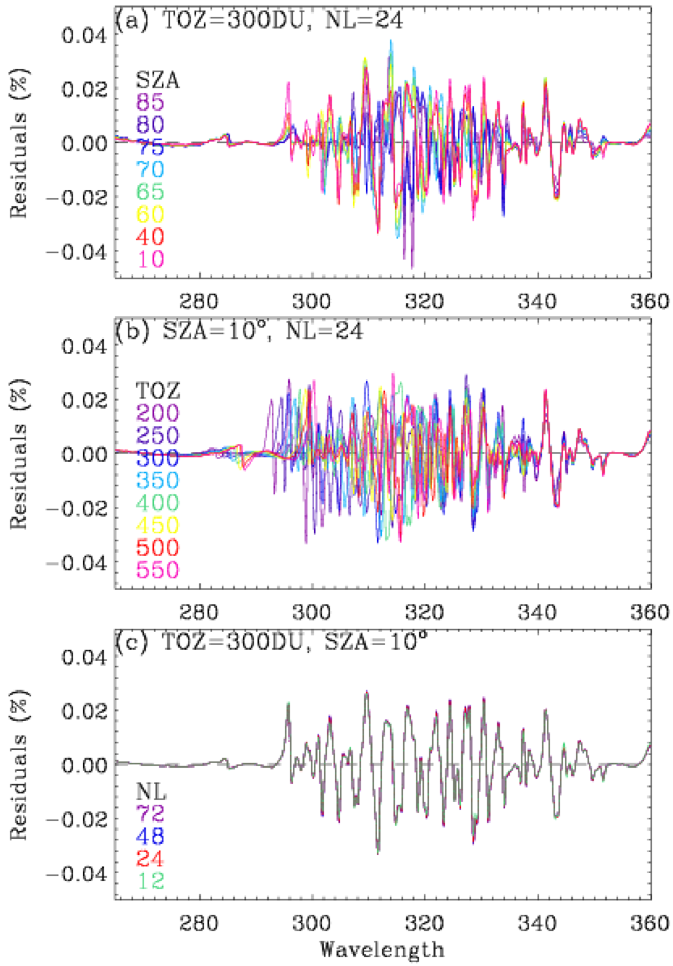

658

659 **Fig. 6**. Residuals (%) of the PCA-RT radiances with the binning scheme given in Table 1, for
660 various sets of (a) solar zenith angles, (b) ozone profiles with different total ozone columns
661 (TOZs), and (c) number of atmospheric layers.

662

https://doi.org/10.5194/amt-2020-349
Preprint. Discussion started: 18 September 2020

Atmospheric Measurement Techniques
Discussions

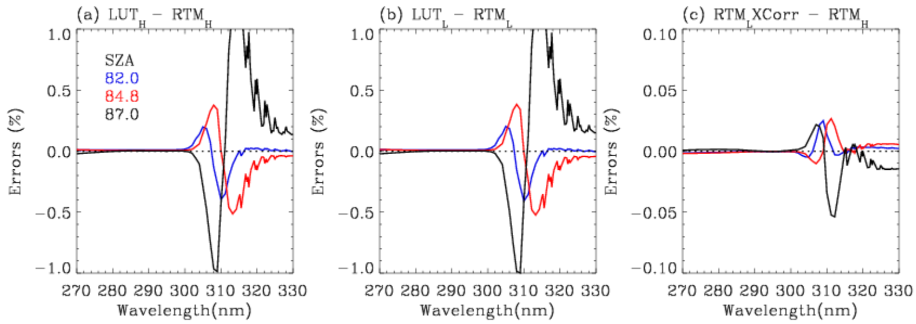

Fig. 7. Evaluation of simulations with respect to extreme SZAs at VZA = 61°, AZA = 0 °, ALB=0 %, and surface pressure = 1013.25 hPa. LUT and RTM represent LUT and on-line radiative transfer model (RTM) based calculations, respectively, with the subscripts H and L indicating high and low accuracy configurations. RTM_L X Corr radiances are simulated using on-line RTM with low accuracy configuration, but corrected using LUT_H/LUT_L.

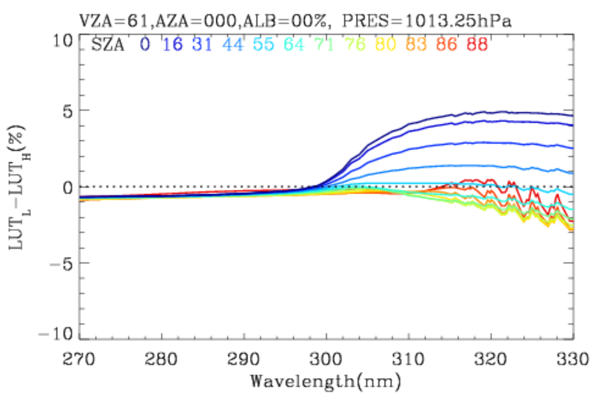

Fig. 8. Example of LUT-based correction spectrum.

https://doi.org/10.5194/amt-2020-349
Preprint. Discussion started: 18 September 2020

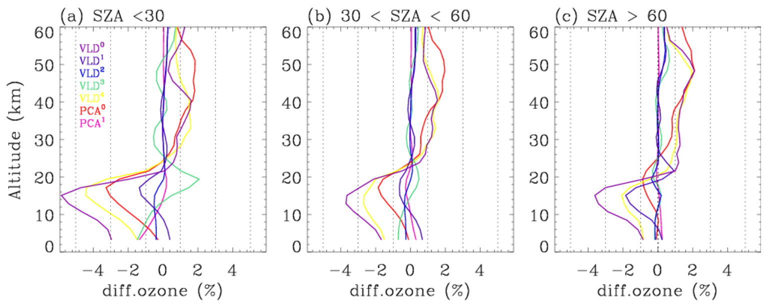

Fig. 9. Mean biases of ozone profile retrievals with different configurations compared to those with the reference configuration. Each configuration is given in Table 4.

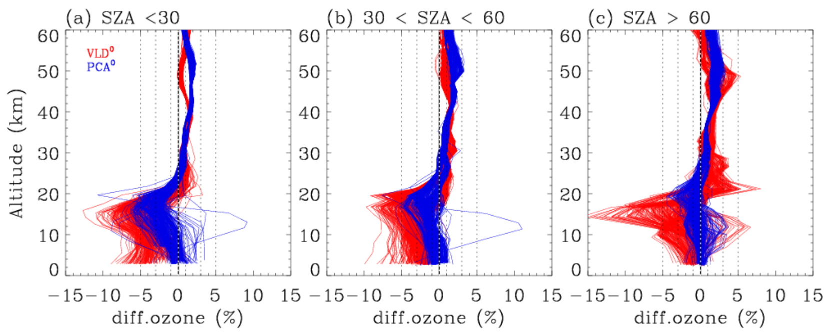

Fig. 10. Same as Fig.9, but for individual differences. VLD^0 and PCA^0 represent v1 and v2 forward model configurations, respectively.

https://doi.org/10.5194/amt-2020-349
Preprint. Discussion started: 18 September 2020

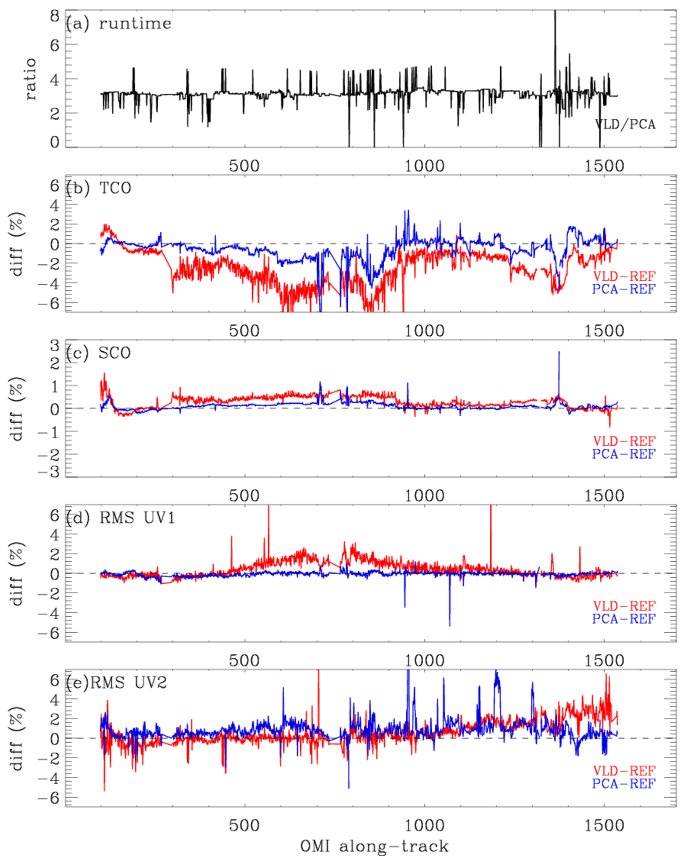

Fig. 11. Same as Fig. 10, but for (a) runtime, (b) tropospheric column ozone (TCO), (c) stratospheric column ozone (SCO), and (d) UV1 (270-310 nm)/(e) UV2 (310-330 nm) fitting residuals, along with the OMI along-track position (1-1644) at nadir cross-track. Note that the fitting residuals are estimated as root mean square (RMS) errors for differences between measured and simulated spectra relative to the measurement error. VLD and PCA represent v1 and v2 forward model configurations, respectively.